Electronic Supplementary Material (ESI) for Journal of Materials Chemistry A.

Supplementary Information

# Interfacial Electron Transfer of Heterostructure MIL-88A/Ni(OH)$_2$ Enhances Oxygen Evolution Reactions in Alkaline Solutions

*Zhengxin Qian,[a] Keke Wang,[a] Kexin Shi,[a] Zhaoqin Fu,[a] Zequn Mai,[b] Xiufang Wang,[a] Zhenghua Tang,[*,b,c] and Yong Tian[*,a]*

[a] School of Pharmacy, Guangdong Pharmaceutical University, Guangzhou, 510006, P. R. China

[b] Guangzhou Key Laboratory for Surface Chemistry of Energy Materials, New Energy Research Institute, School of Environment and Energy, South China University of Technology, Guangzhou Higher Education Mega Center, Guangzhou, Guangdong 510006, P. R. China.

[c] Guangdong Engineering and Technology Research Center for Surface Chemistry of Energy Materials, School of Environment and Energy, South China University of Technology, Guangzhou Higher Education Mega Centre, Guangzhou 510006, P. R. China.

## Detailed Calculation of EASA and TOF Values

The electrochemically active surface area (EASA) value was estimated from the electrochemical double-layer capacitance ($C_{dl}$) of the catalyst. $C_{dl}$ was measured via cyclic voltammograms with a potential range where no apparent Faradaic process was taking place. The double-layer charging current $I_C$ can be related to the scan rates through Eq. S1:

$$I_C = C_{dl} \times v \qquad \text{(S1)}$$

Thus, plotting the charging currents at a specific potential against various scan rates leads to a straight line with the slope equal to $C_{dl}$. Subsequently, the EASA value can be obtained by Eq. S2:

$$\mathrm{EASA} = C_{dl} / C_S \qquad \text{(S2)}$$

where $C_S$ is the capacitance measured from ideally smooth, planar surfaces of the catalyst, and here the typical value of 0.040 mF $cm^{-2}$ for Ni is used for calculation.

Turnover frequency (TOF) calculation: The turnover frequency (TOF) value is calculated according to the Eq. S3:

$$TOF = (j \times A) / (4 \times F \times n) \qquad \text{(S3)}$$

Where j is the current density at an overpotential (η) of 370 mV. A is the geometric area of the electrode (1 $cm^2$ for the active area in this work). F is the faraday constant (96485 C/mol). n is the number of moles of the active materials that are integrated on carbon cloth. n = m/M, m is the mass of active material on carbon cloth; M is the molecular weight of the corresponding active material. All the Ni atoms and Fe atoms were assumed to be accessible for OER catalysis. The content of Fe and Ni in active material was determined by Inductively Coupled Plasma-Atomic Emission Spectroscopy (ICP-AES).

## Detailed Calculation of Density Functional Theory

The DFT calculation is conducted using Materials Studio 2017 application software and CASTEP package as the main modules. The exchange correlation function is Spin-Polarized Perdew-Burke Ernzerhof (PBE) of the Generalized Gradient Approximation (GGA) with Koelling-Hamon relativistic treatment and spin polarization assumption and in numerical optimization Broyden–Fletcher–Goldfarb Shanno (BFGS) was employed which is an iterative method for solving unconstrained nonlinear optimization problems.[1, 2]

The interaction between valence electrons and ion nuclei is described in terms of On-The-Fly-Generated (OTFG) ultra-soft pseudopotential, which appears in the CASTEP code to generate pseudo-potential dynamically. The base set defined by the energy cutoff value is one of the most important parameters to determine the accuracy of CASTEP calculation. In this work, the cutoff energy of 480 eV and a k-point set grid (2*2*1) were employed as parameters to optimize the geometry of MIL-88A(001) and $Ni(OH)_2$(001) structures.[3, 4] For this calculation, the threshold for self-consistent field iterations (SCF) is $2.0*10^{-6}$ eV per atom, the convergence tolerance parameters of the optimized calculation are the total energy of $2.0*10^{-5}$ eV per atom, maximum force of 0.05 eV/Å and maximum displacement of $2.0*10^{-3}$ Å for both MIL-

88A(001) and $Ni(OH)_2$(001) structures.[5, 6] $Ni(OH)_2$ (a = b = 3.161 Å, c = 4.602 Å) crystal has a space group of Hermann Mauguin P3m1 (156) and the space group of MIL-88A (a = b = 11.184 Å, c = 14.591 ) is P-62 c. The 001 surface is simulated by cutting the optimized crystals along (001) direction (cleavage plane (h k l) value of (001)). A supercell containing (7*7) $Ni(OH)_2$ (001) slab and 2*2 MIL-88A(001) slab at least 15 Å vacuum space was used in the calculation, and a layer is built as the surface with a vacuum of 15 Å to avoid periodic interactions.[6]

Adsorption Locator is designed for the study of individual systems, allowing us to find low energy adsorption sites on both periodic and nonperiodic substrates or to investigate the preferential adsorption of mixtures of adsorbate components. A low energy adsorption site is identified by carrying out a Monte Carlo search of the configurational space of the substrate-adsorbate system. After the surface is prepared it is allowed to relax by using the optimizing parameters used above in the geometry optimization and adsorption energy of the substrate structure, the MIL-88A(001), $Ni(OH)_2$ (001) and the heterostructure layer using $OH^-$ as adsorbent is determined.[7]

**Table S1.** Fitting parameters obtained from the EIS data for the OER in 1 M KOH.

| Catalyst | Rs (Ω) | $R_1$ (Ω) | $CPE_1$-T (F) | $CPE_2$-P | $R_2$ (Ω) | $CPE_2$-T (F) | $CPE_2$-P |
|---|---|---|---|---|---|---|---|
| MIL-88A/CC | 2.361 | 10.96 | 0.4688 | 0.0258 | 153.7 | 0.0105 | 0.8517 |
| $Ni(OH)_2$/CC | 3.326 | 1.28 | 0.0112 | 0.9197 | 12.2809 | 0.0256 | 0.7958 |
| MIL-88A/$Ni(OH)_2$-CC | 2.14 | 0.023 | 0.1326 | 0.3607 | 5.138 | 0.2412 | 0.8817 |
| $RuO_2$/CC | 2.57 | 1.56 | 0.0061 | 0.5771 | 8.659 | 0.0155 | 0.8530 |

Rs: electrolyte resistance.

$R_1$: charge-transfer resistance.

$R_2$: solid−electrolyte interface resistance.

$CEP_1$: capacitance generated from the Faradic process, and constant-phase element.

$CEP_2$: capacitance arisen from the solid−electrolyte interface process.

**Table S2.** Fitting parameters obtained from the EIS data for the OER in 0.1 M KOH.

| Catalyst | Rs (Ω) | $R_1$ (Ω) | $CPE_1$-T (F) | $CPE_2$-P | $R_2$ (Ω) | $CPE_2$-T (F) | $CPE_2$-P |
|---|---|---|---|---|---|---|---|
| MIL-88A/CC | 10.83 | 19.08 | 0.0094 | 0.8351 | 185.2 | 0.0026 | 0.7210 |
| $Ni(OH)_2$/CC | 9.294 | 3.234 | 0.0274 | 0.5198 | 32.8 | 0.0048 | 0.9466 |
| MIL-88A/$Ni(OH)_2$-CC | 10.07 | 2.036 | 0.0535 | 0.5013 | 16.64 | 0.0348 | 0.8223 |
| $RuO_2$/CC | 10.24 | 6.77 | 0.0370 | 0.8647 | 26.25 | 0.0039 | 0.6534 |

Rs: electrolyte resistance.

$R_1$: charge-transfer resistance.

$R_2$: solid−electrolyte interface resistance.

$CEP_1$: capacitance generated from the Faradic process, and constant-phase element.

$CEP_2$: capacitance arisen from the solid−electrolyte interface process.

**Table S3.** A comparison of the OER activity of MIL-88A/Ni(OH)$_2$-CC with recently reported the most top-level electrocatalysts.

| **Catalysts** | **Electrolyte** | **Overpotential (mV)** | **$C_{DL}$ (mF)** | **Reference** |
|---|---|---|---|---|
| MIL-88A/Ni(OH)$_2$-CC | 1.0 M KOH | 250<br>@10 mA cm$^{-2}$ | 19.5 | This work |
| MIL-88A/Ni(OH)$_2$-CC | 0.1 M KOH | 352<br>@10 mA cm$^{-2}$ | - | This work |
| HOF-Co$_{0.5}$Fe$_{0.5}$/NF | 1.0 M KOH | 278<br>@10 mA cm$^{-2}$ | 4.10 | [8] |
| MAF-X27-OH/Cu foil | 1.0 M KOH | 338<br>@10 mA cm$^{-2}$ | - | [9] |
| CoO$_x$-ZIF | 1.0 M KOH | 318<br>@10 mA cm$^{-2}$ | 3.04 | [10] |
| NiFe-MOF/NF | 1.0 M KOH | 240<br>@10 mA cm$^{-2}$ | - | [11] |
| Ni$_{0.75}$V$_{0.25}$-LDH | 1.0 M KOH | 350<br>@27 mA cm$^{-2}$ | 0.27 | [12] |
| Co$_3$O$_4$C-NA | 0.1 M KOH | 290<br>@10 mA cm$^{-2}$ | 209.7 | [13] |
| Co-CNT/PC | 0.1 M KOH | 315<br>@10 mA cm$^{-2}$ | - | [14] |

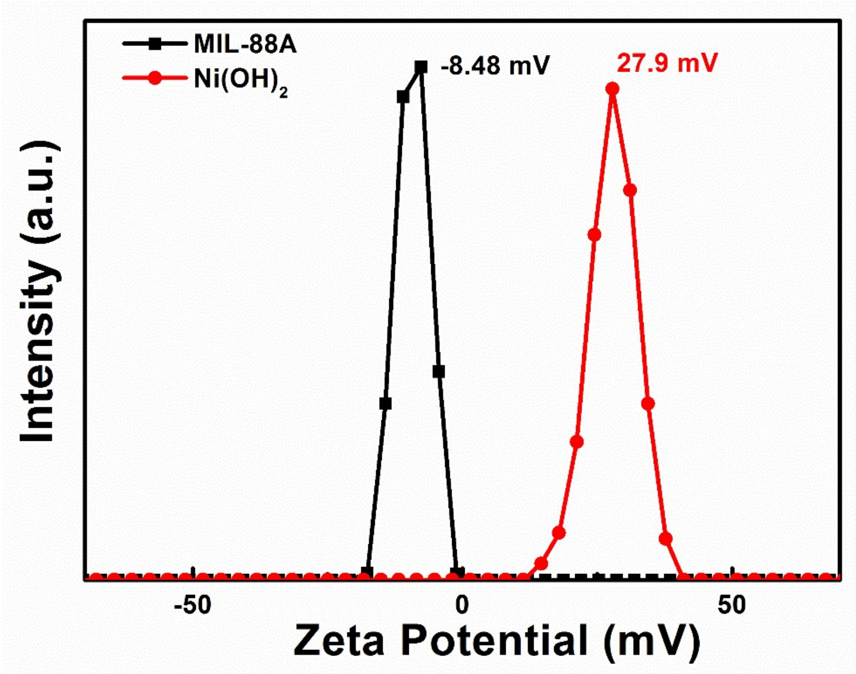

**Figure S1.** The Zeta potential measurement of MIL-88A only and $Ni(OH)_2$ only.

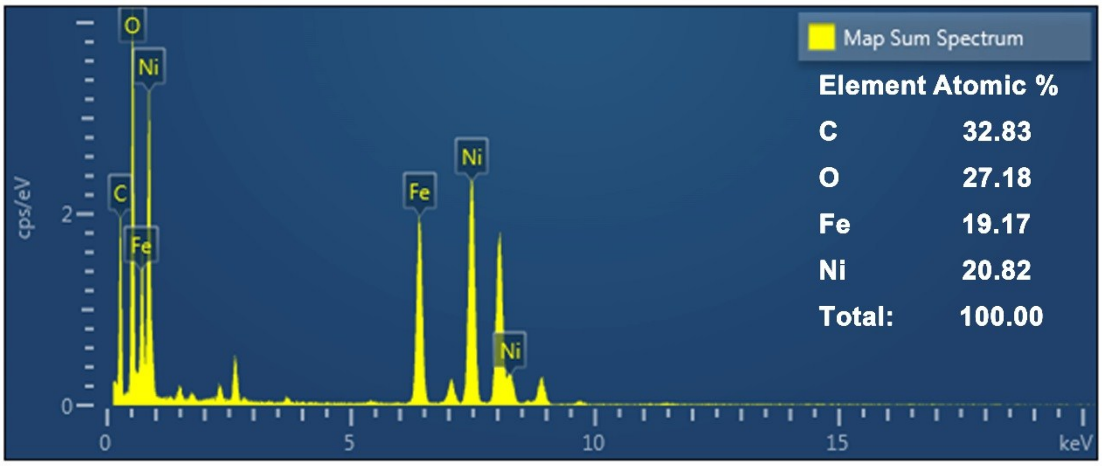

| Element | Atomic % |
|---|---|
| C | 32.83 |
| O | 27.18 |
| Fe | 19.17 |
| Ni | 20.82 |
| Total: | 100.00 |

**Figure S2.** EDS spectrum of MIL-88A/$Ni(OH)_2$-CC (The rest of the signals are from the Cu substrate).

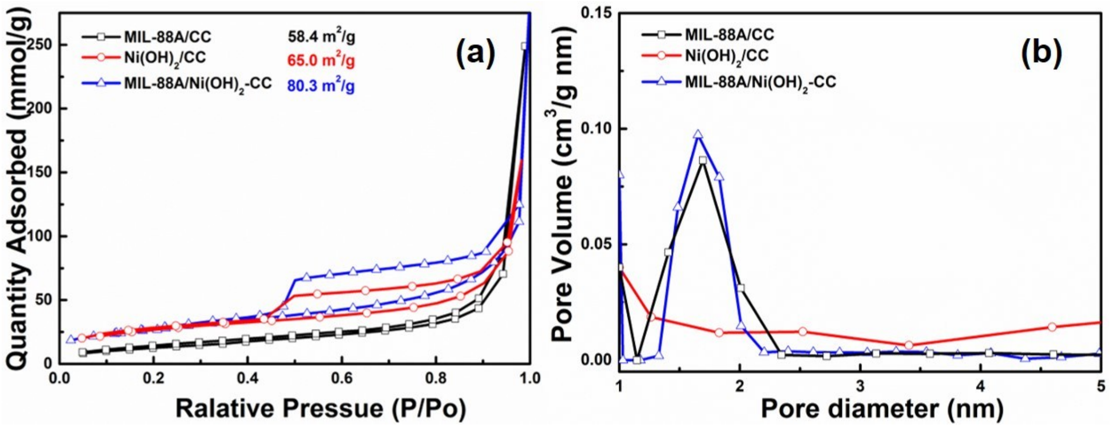

**Figure S3.** (a) $N_2$ adsorption/desorption isotherms and (b) corresponding pore-size distribution of MIL-88A/CC, $Ni(OH)_2$/CC, and MIL-88A/$Ni(OH)_2$-CC.

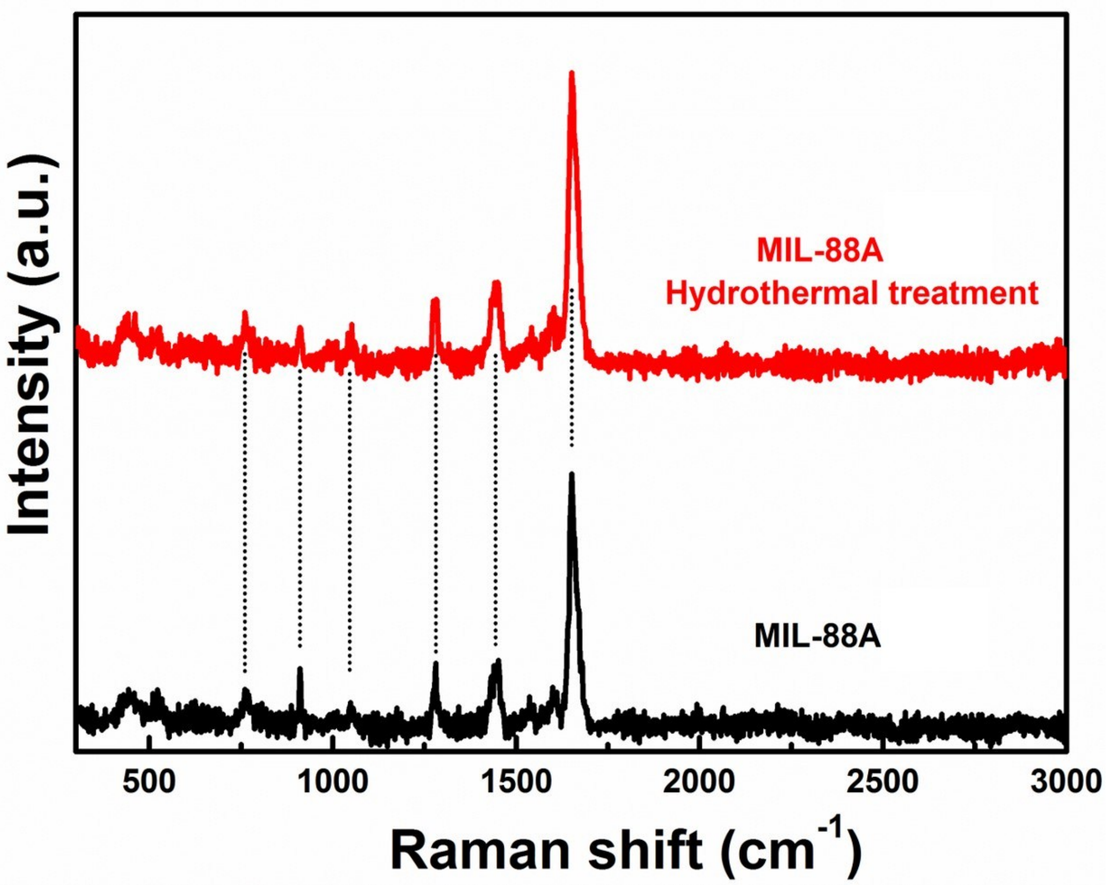

**Figure S4.** The Raman spectra of MIL-88A before and after the hydrothermal reaction.

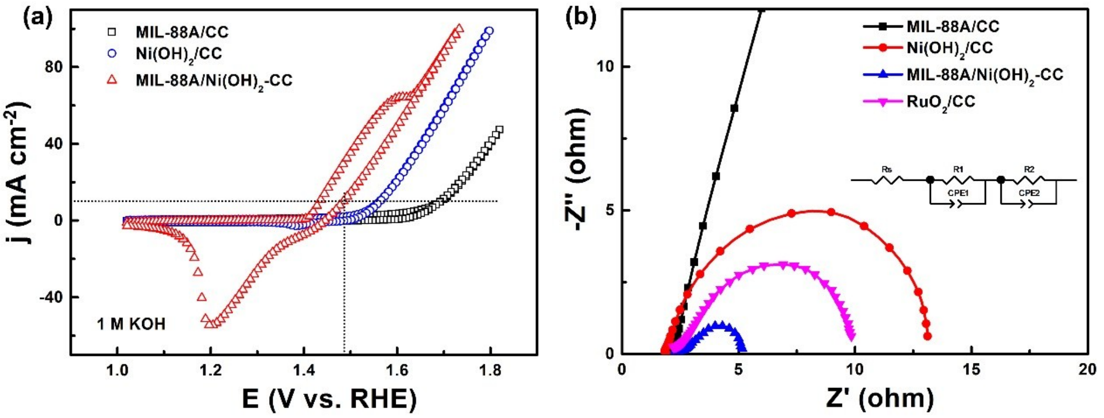

**Figure S5.** (a) The CV curves of MIL-88A/CC, Ni(OH)$_2$/CC, and MIL-88A/Ni(OH)$_2$-CC in 1 M KOH solution with reversed sweep direction and corresponding (b) EIS diagrams at an applied potential of 1.50 V (Inset shows the fitting results).

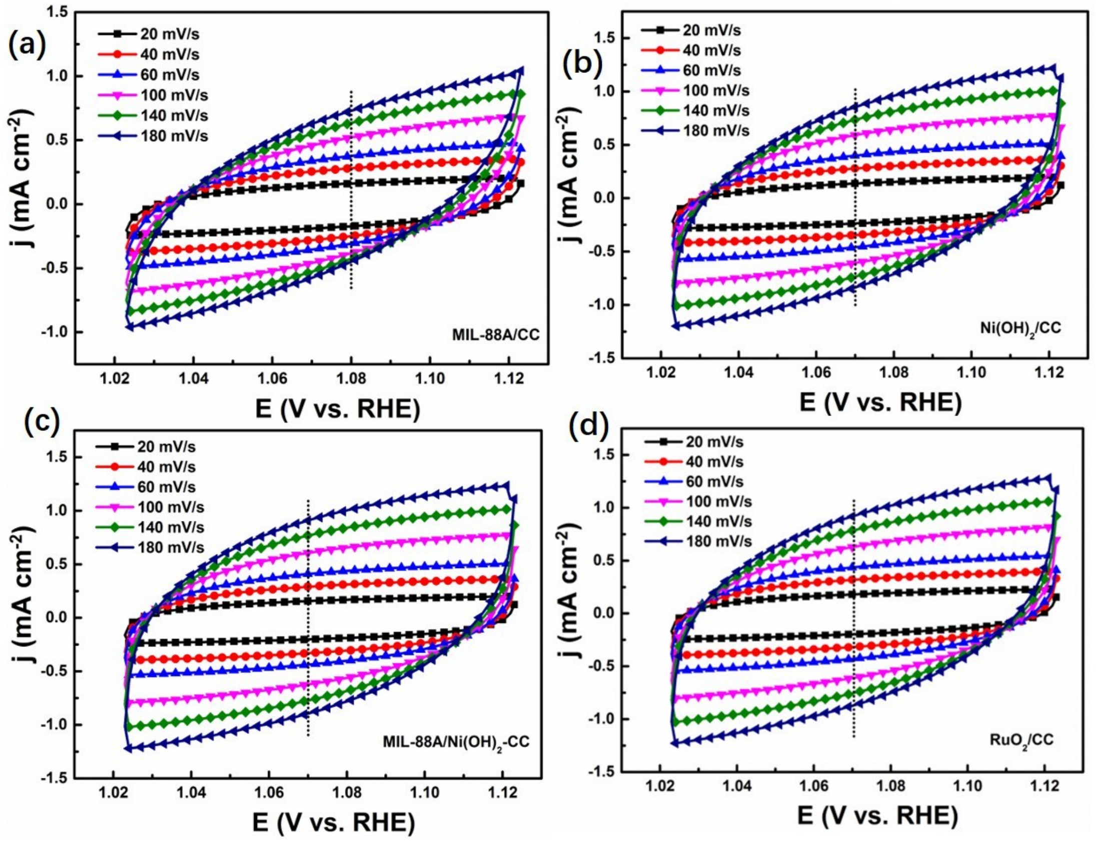

**Figure S6.** The CV curves of (a) MIL-88A/CC, (b) $Ni(OH)_2$/CC, and (c) MIL-88A/$Ni(OH)_2$-CC modified carbon cloth electrode in the double layer region at scan rates of 20, 40, 60, 100, 140, and 180 mV $s^{-1}$ in 1.0 M KOH. By plotting the capacitive currents ($J_{anodic}$ - $J_{cathodic}$) versus scan rate, the capacitance can be estimated as half of the slope.

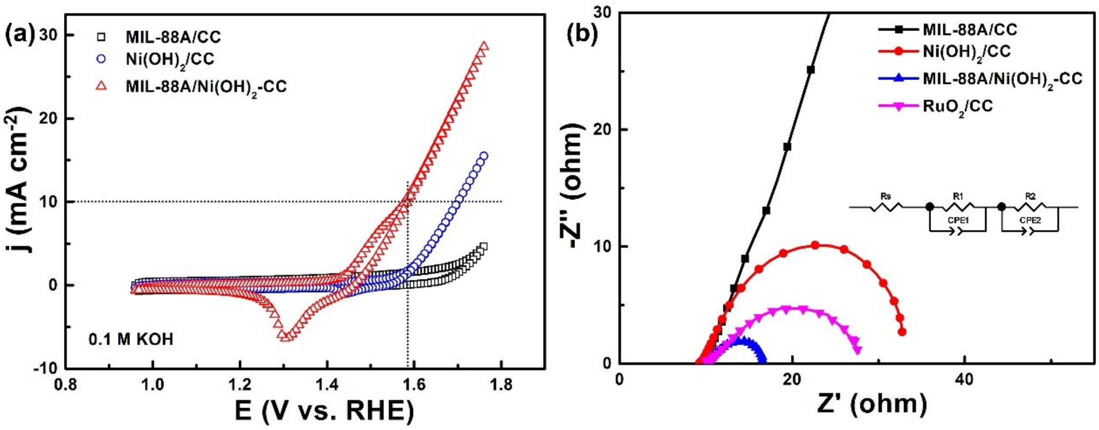

**Figure S7.** (a) The CV curves of MIL-88A/CC, Ni(OH)$_2$/CC, and MIL-88A/Ni(OH)$_2$-CC in 0.1M KOH solution and corresponding (b) EIS diagrams at an applied potential of 1.55 V (Inset show the fitting results).

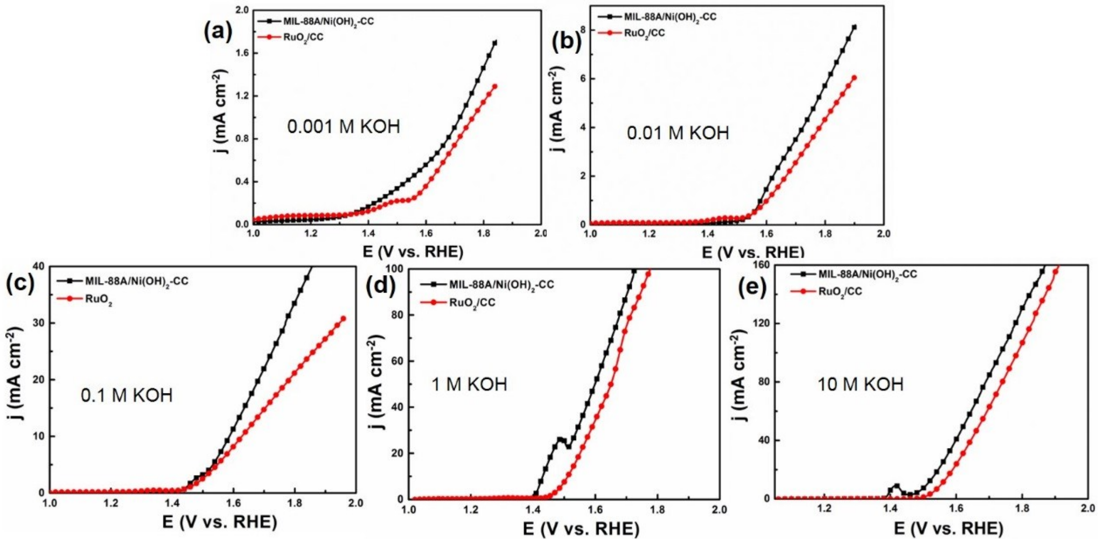

**Figure S8.** The polarization curves of MIL-88A/Ni(OH)$_2$ and RuO$_2$/CC at different concentrations of KOH in 0.001 M, 0.01 M, 0.1 M, 1 M and 10M, respectively.

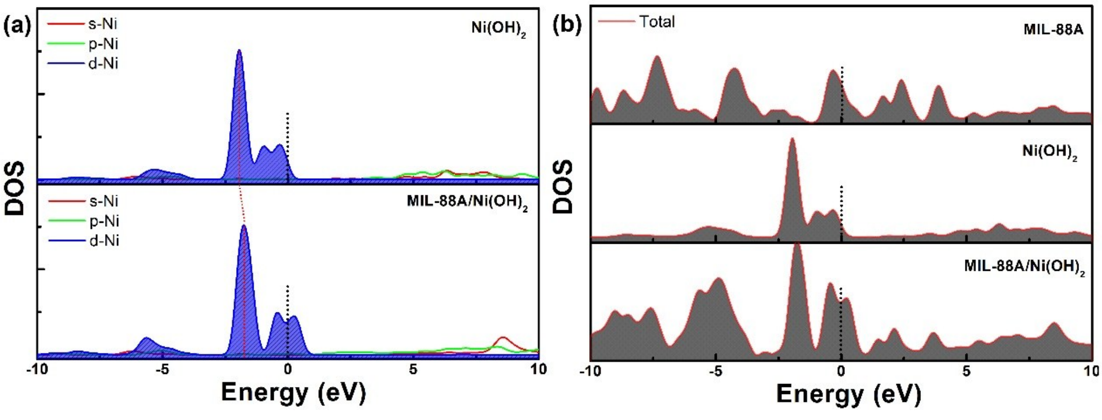

**Figure S9.** (a) The density of states of Ni(OH)$_2$ and MIL-88A/Ni(OH)$_2$, where the red, green, and blue lines represent the contributions of the s, p, and d orbitals of Ni atoms in DOS. (b) The total density of states of the three samples.

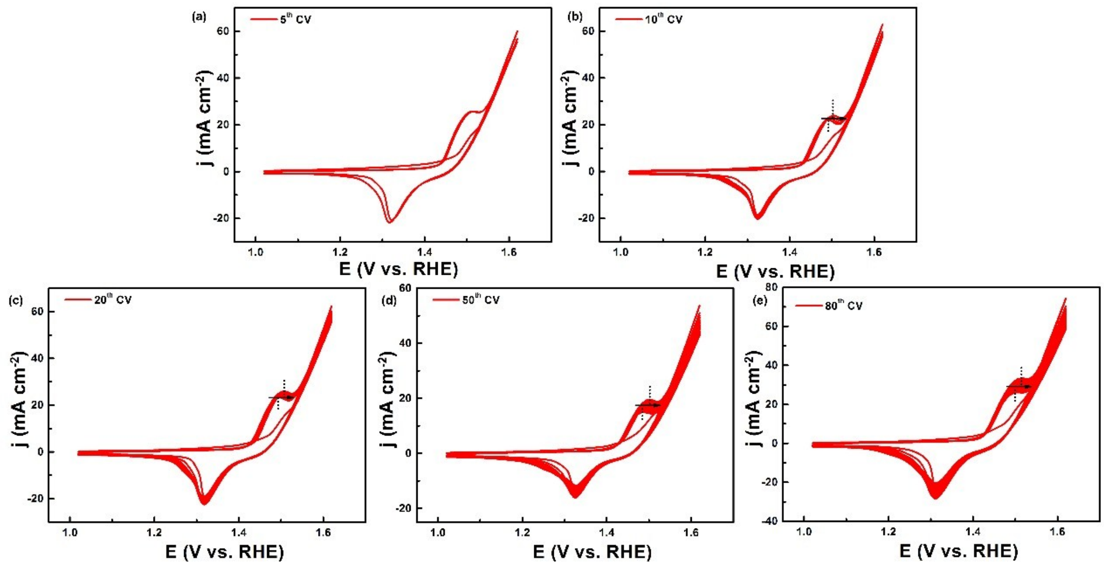

**Figure S10.** The CV curves of MIL-88A/Ni(OH)$_2$-CC under different cycle numbers of 5, 10, 20, 50, and 80 in 1.0 M KOH. The oxidation peaks with different cycles all moved to higher potentials continuously.

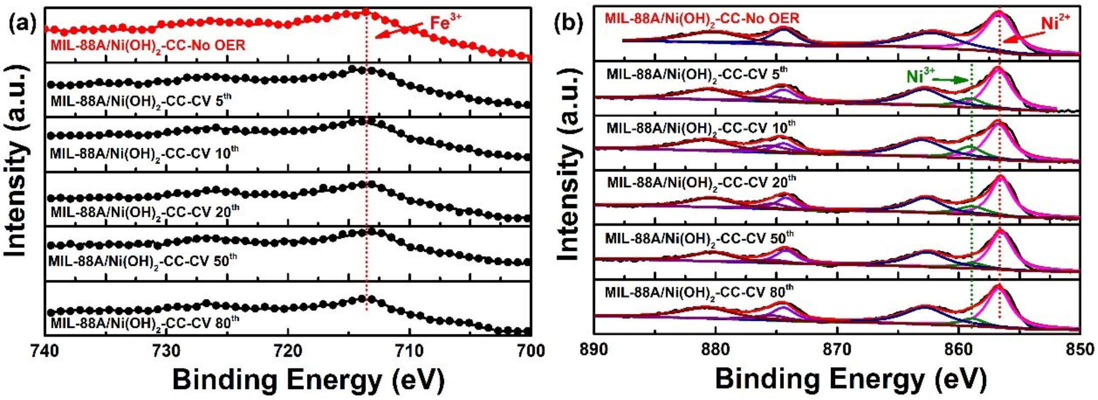

**Figure S11.** (a) The core-level XPS spectra of the Fe 2p electrons and (b) the Ni 2p electrons for MIL-88A/Ni(OH)$_2$-CC after different CV cycle numbers of 5, 10, 20, 50, and 80.

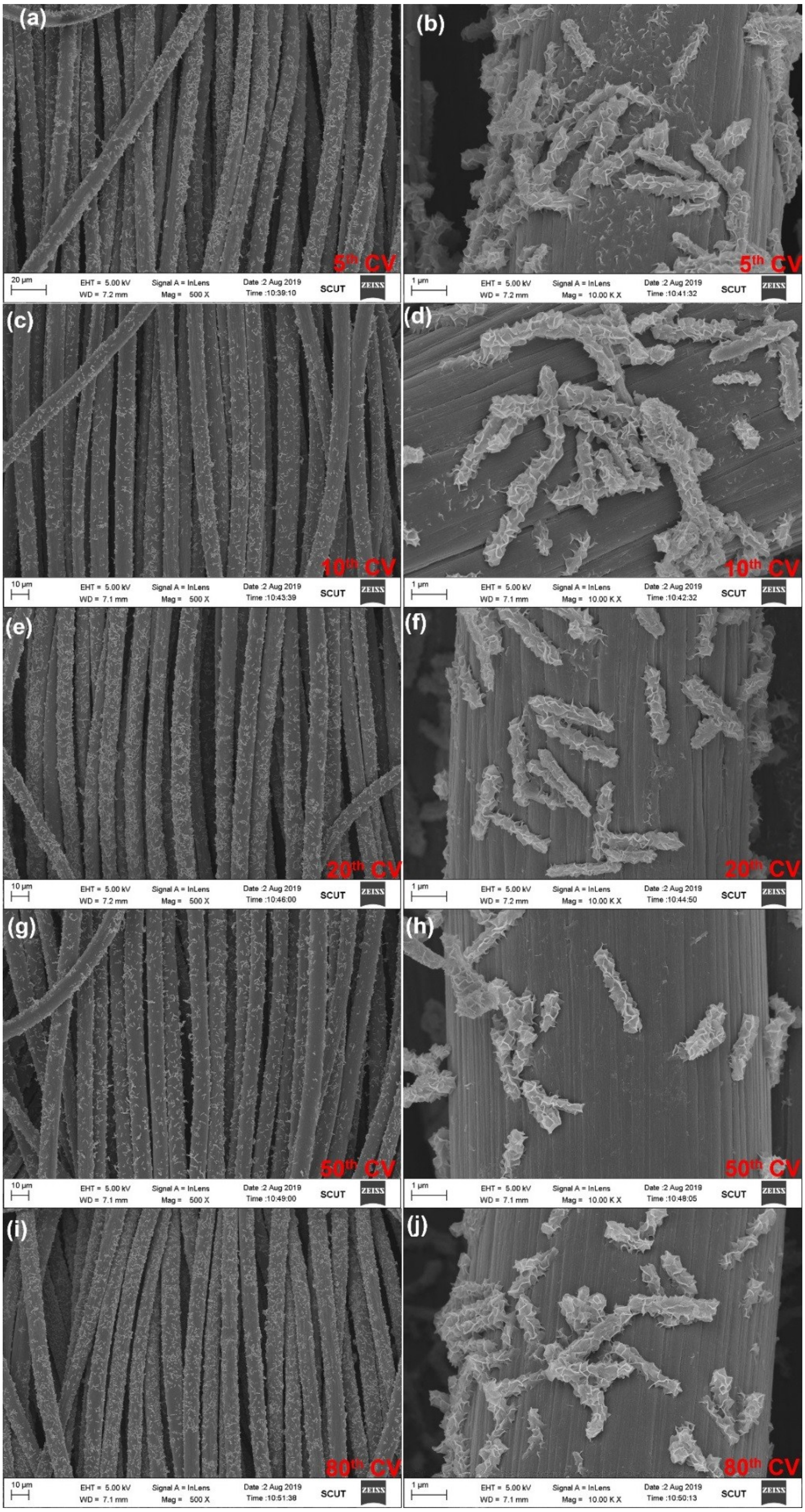

**Figure S12.** The SEM of MIL-88A/Ni(OH)$_2$-CC after different CV cycle number of 5, 10, 20, 50, and 80.

## References

1. J. P. Perdew, K. Burke and M. Ernzerhof, *Phys. Rev. Lett.*, 1996, **77**, 3865-3868.
2. D. Vanderbilt, *Phys. Rev. B*, 1990, **41**, 7892-7895.
3. H. J. Monkhorst and J. D. Pack, *Phys. Rev. B*, 1976, **13**, 5188-5192.
4. M. C. Payne, M. P. Teter, D. C. Allan, T. A. Arias and J. D. Joannopoulos, *Rev. Modern Phys.*, 1992, **64**, 1045-1097.
5. M. D. Segall, P. J. D. Lindan, M. J. Probert, C. J. Pickard, P. J. Hasnip, S. J. Clark and M. C. Payne, *J. Phys. Condensed Matter*, 2002, **14**, 2717-2744.
6. J. Clark Stewart, D. Segall Matthew, J. Pickard Chris, J. Hasnip Phil, I. J. Probert Matt, K. Refson and C. Payne Mike, *Journal*, 2005, **220**, 567.
7. K. He, T. Tadesse Tsega, X. Liu, J. Zai, X.-H. Li, X. Liu, W. Li, N. Ali and X. Qian, *Angew. Chem., Int. Ed.*, 2019, **58**, 11903-11909.
8. F. Q. Liu, J. W. Liu, Z. Gao, L. Wang, X.-Z. Fu, L. X. Yang, Y. Tao, W. H. Yin and F. Luo, *Appl. Catal. B: Environ.*, 2019, **258**, 117973.
9. X.-F. Lu, P.-Q. Liao, J.-W. Wang, J.-X. Wu, X.-W. Chen, C.-T. He, J.-P. Zhang, G.-R. Li and X.-M. Chen, *J. Am. Chem. Soc.*, 2016, **138**, 8336-8339.
10. S. Dou, C.-L. Dong, Z. Hu, Y.-C. Huang, J.-l. Chen, L. Tao, D. Yan, D. Chen, S. Shen, S. Chou and S. Wang, *Adv. Funct. Mater.*, 2017, **27**, 1702546.
11. J. Duan, S. Chen and C. Zhao, *Nat. Commun.*, 2017, **8**, 15341.
12. K. Fan, H. Chen, Y. Ji, H. Huang, P. M. Claesson, Q. Daniel, B. Philippe, H. Rensmo, F. Li, Y. Luo and L. Sun, *Nat. Commun.*, 2016, **7**, 11981.
13. T. Y. Ma, S. Dai, M. Jaroniec and S. Z. Qiao, *J. Am. Chem. Soc.*, 2014, **136**, 13925-13931.
14. S. Dou, X. Li, L. Tao, J. Huo and S. Wang, *Chem. Commun.*, 2016, **52**, 9727-9730.